






Cluster decay half-lives of $^{112-122}\text{Ba}$ isotopes from the ground state and intrinsic excited state using the relativistic mean-field formalism within the preformed-cluster-decay model

Joshua T. Majekodunmi ^{1,*}, M. Bhuyan ^{2,†}, D. Jain ³, K. Anwar ¹, N. Abdullah ¹ and Raj Kumar ^{4,‡}

¹*Institute of Engineering Mathematics, Faculty of Applied and Human Sciences, Universiti Malaysia Perlis, Arau, 02600, Perlis, Malaysia*

²*Center for Theoretical and Computational Physics, Department of Physics, Faculty of Science, University of Malaya, Kuala Lumpur 50603, Malaysia*

³*Department of Physics, Mata Gujri College, Fatehgarh, Punjab 140407, India*

⁴*School of Physics and Science, Thapar Institute of Engineering and Technology, Patiala, Punjab 147004, India*



(Received 27 August 2021; accepted 15 April 2022; published 26 April 2022)

Background: The cluster radioactivity from the neutron-deficient trans-tin region of the nuclear landscape has given immediate attention in the nuclear structure studies. Recent prediction of the emitting clusters from the ground and intrinsic excited states of proton-rich Ba isotopes opens the direction to explore the corresponding decay characteristics. A theoretical probe is necessary for understanding the cluster decays of Ba isotopes.

Purpose: In the present study, cluster-decay half-lives are calculated and their decay characteristics are investigated for even-even $^{112-122}\text{Ba}$ isotopes in both ground and intrinsic excited states along the proton drip line.

Method: The preformed-cluster-decay model (PCM) is employed for estimating the decay half-lives. The preformation probability (P_0) of the cluster decay from the parent nuclei is calculated by using the well-known phenomenological formula of Blendowske and Walliser [*Phys. Rev. Lett.* **61**, 1930 (1988)], supplemented with the newly proposed Q -value-based preformation factor for the cluster with mass $A_c > 28$. The penetration probability is calculated from the interaction potential using the Wentzel-Kramers-Brillouin (WKB) approximation. The nucleon-nucleon (NN) potential and individual binding energy (BE) of the cluster and daughter nuclei are estimated from the microscopic relativistic mean-field formalism (RMF) and compared with those from experiments and the finite-range-droplet model for the estimation of the Q values of the cluster decays. The nonlinear RMF Lagrangian from which the effective relativistic R3Y NN potential is derived using the NL3* parameter set is employed for the calculation of the nuclear matter densities. The R3Y and well-known M3Y potential are employed to obtain the cluster-daughter interaction potential using the double-folding procedure along with their corresponding RMF densities. The total potential along with their respective cluster decay Q values are used as input in the PCM to obtain the half-lives ($T_{1/2}$) of $^{112-122}\text{Ba}$ isotopes in their ground and intrinsic excited states.

Results: The calculated half-lives ($T_{1/2}$) for relativistic R3Y NN potential and Q values are found to deviate slightly compared to the ones from the M3Y due to the difference in their barrier characteristics. We notice that at elongated neck configuration a minimum neck-length parameter $\Delta R = 1.0$ fm is required for R3Y potential due to its repulsive nature, whereas the value is 0.5 fm is suitable for the M3Y case. However, the estimated decay half-lives for both the potentials are in reasonably good agreement with the experimental lower limit of ^{114}Ba . In contrast with the ground-state decays, the inclusion of intrinsic excitation reduces the corresponding half-life values considerably but does not rule out the role of magicity.

Conclusions: The sensitivity of the decay half-lives to Q values and neck-length parameter has also been demonstrated. The decay half-lives are predicted for various cluster decays from neutron-deficient Ba isotopes. Since none of the experimental half-lives for the examined clusters is precisely known yet, further studies with available observed half-lives will be needed to substantiate our findings.

DOI: [10.1103/PhysRevC.105.044617](https://doi.org/10.1103/PhysRevC.105.044617)

I. INTRODUCTION

Unstable nuclei are characterized by the spontaneous disintegration of α and β particles and γ rays

in a process known as nuclear radioactivity. Other than these three major emissions, there exists another decay mode between α decay and spontaneous fission commonly called cluster radioactivity: a spontaneous disintegration and/or decay of radioactive nuclei where certain clusters heavier than ^4He are emitted. After its first prediction by Sandulescu *et al.* [1], the cluster radioactivity was investigated experimentally by Rose and Jones to validate the emission of ^{14}C from radium-223

*majekjoe1@gmail.com

†bunuphy@um.edu.my

‡rajkumar@thapar.edu

[2]. Since then, this discovery has led to a large number of experimental and theoretical attempts to understand the physics of cluster emissions from the heavy nuclei [3–7]. Consequently, about 30 more radioactive decays that range from light to heavy clusters, ^{14}C to ^{34}Si , has been discovered [8]. The decays of trans-lead parents nuclei emitting clusters are marked with long partial half-lives ($T_{1/2}$) in the range 10^{11} – 10^{30} s. The ^{34}Si emitted from ^{238}U is the heaviest cluster observed experimentally, having the largest measured half-life ($\log_{10} T_{1/2}$) of 29.04 s [8]. The clusters of ^{46}Ar and $^{48,50}\text{Ca}$ are emitted with unknown precise half-life from ^{252}Cf , although their lower limit is available in Refs. [9,10]. In cluster radioactive decay, the emitted clusters are usually associated with doubly magic daughters (closed-shell) or neighbors. Notably, this has a great consequence on the shell effects, especially as it relates to the cluster radioactivity half-lives [11–13].

Besides the cluster emissions of neutron-rich nuclei in the trans-lead region, two other known islands of cluster emissions are studied via various models [12,14–19]. The first one is the superheavy island [14–17] and the second is the trans-tin region [12,18,19] from which the decay yield daughters in the neighborhood of ^{100}Sn . Several notable experimental attempts in this direction were made [20–23] but lack precise measurement of half-lives (for example, in ^{12}C decay of ^{114}Ba) in the ground state, proffering only upper and lower limits. An alternative to these experimental uncertainties is the theoretical approach, which has been used substantially to investigate the cluster radioactive decay process [24–28]. The cluster decay models are broadly categorized into two categories based on how they treat the cluster emission, viz. the fission- and α -decay-like models. The former assumes that cluster formation takes place during the deformation and separation process of the parent nucleus while penetrating the confining interaction barrier, e.g., the analytic super asymmetric fission model (ASAFM) of Poenaru *et al.* [29,30], which involves the fitting of the model constants to sizable data on α -decay half-lives and ^{14}C cluster emission from ^{223}Ra . The description of cluster radioactivity such as superasymmetric fission within the mean-field approach can be found in Refs. [31–33]. The latter one comes from the assumption of natural birth, i.e., the clusters are assumed to be preborn (performed) within the parent nuclei [25,34–38]. It incorporates the spectroscopic or preformation factor P_0 which assimilates the structural properties of the decaying parent nucleus.

The preformed-cluster-decay model (PCM) of Gupta and collaborators [7,39,40] is employed for the study of the ground and intrinsic excited state cluster radioactivity of neutron-deficient nuclei from the trans-tin region. It is worth mentioning that the PCM originates from the well-known quantum mechanical fragmentation theory (QMFT), where the Gamow theory of α decay is employed [41,42]. The description assumes that clusters are preformed within the parent nuclei are composed of numerous nucleons tunneling through the interaction barrier formed by the superposition of nuclear and Coulomb potentials [43,44]. The Coulomb potential is well known, whereas different phenomenological and microscopic approaches are established to determine the nuclear

potential [45–50]. Thus, for a better understanding of the decay phenomena, the choice of nuclear potential is crucial. At low energy, it is assumed that the interaction potential between two nucleons is instantaneous, being substantiated by the theory of nuclear force, and is relevant for the nuclear structure calculations [46,51,52]. Recently, the R3Y nucleon-nucleon (NN) potential in parallel with the phenomenological M3Y [53] from the relativistic mean-field (RMF) Lagrangian is applied for the study of cluster radioactivity [24,54]. Furthermore, the refitted version of the popular NL3 parameter set, namely, NL3*, has gained considerable application for its successful description of both ground and excited state bulk properties of the exotic nuclei [55–63]. Hence, it will be interesting to apply the nuclear interaction potential from R3Y NN potential and corresponding mean-field densities for NL3* parameter set.

The existing cluster(s) from the ground and intrinsic excited states of neutron-deficient Ba isotopes, which were predicted by showing the internal configuration of matter density distribution using the relativistic mean-field model by Bhuyan *et al.* [36], opens the direction to explore their corresponding decay characteristics. In other words, the cluster decay properties such as their Q values and corresponding half-lives are examined within the relativistic mean-field formalism for possible identified clusters from 112 – ^{122}Ba nuclei in their ground states (g.s.), intrinsic first (1st) and second excited states (2nd e.s.), namely ^9C , ^{12}C , ^{13}O , $^{12,14}\text{N}$, $^{17,18}\text{Ne}$, ^{35}Cl , ^{36}Ar , and $^{42,43}\text{Ca}$. It is worth mentioning that to the best of our knowledge, for the first time we have studied the emitting ground state cluster and daughter from the excited state of parent nuclei within the relativistic mean-field formalism, as predicted in Ref. [36]. The ingredients of PCM, i.e., the preformation probability (P_0) and penetration probability (P) are evaluated by employing well-known phenomenological formula of Blendowske and Walliser [64] supplemented with the Q value based formula [65,66] and WKB approximation [67–69], respectively. For estimating the Q values of the cluster decay, in addition to the binding energies obtained from RMF (NL3*), the experimental [70], and finite-range-droplet Model (FRDM) [71] values are also employed for the comparison. The relative separation distance between two fragments or clusters is accounted for by the neck parameter ΔR which assimilates the neck formation effect and determines the first turning point of the barrier penetration. The respective predictions are also compared with the parallel calculation done for the well-known M3Y NN potential [53]. As such, this study can provide helpful information for future experiments on the cluster decay of various nuclei in this mass region. Our present calculations are limited to the spherical coordinate system to deduce NN interaction potential.

Section II A describes the relativistic mean-field formalism and the total interaction potential using the double-folding procedure for R3Y and M3Y NN potential using densities of daughter and cluster. A concise description of the PCM is also presented in this section. The results of our calculations are shown and discussed in Sec. III. Based on the inferences drawn from the study, Sec. IV gives the summary and conclusion.

II. METHODOLOGY

The present calculations can be grouped into two parts. First, the R3Y nucleon-nucleon (NN) interaction potential and the folded cluster-daughter densities (ρ_c and ρ_d) are solely obtained from the relativistic mean-field (RMF) formalism. This procedure is repeated for the well-known M3Y NN potential for the sake of comparison. Likewise, the Q value is a necessary input for the reaction process. Hence, the second part is aimed at calculating the half-lives from the preformed-cluster-decay model (PCM) for which the Q value (for each reaction system) is deduced from the RMF approach. Again, for comparison in this second procedure, the Q values for the systems under study are also estimated from the microscopic-macroscopic FRDM and the experimental binding energy data. A brief description of the relativistic mean-field approach and double-folding method for calculating NN potential and PCM for estimating the cluster decay half lives are discussed in this section.

A. Relativistic mean-field approach

The nonlinear relativistic mean-field Lagrangian density that describes the interaction between the many-body system of nucleons and mesons is expressed as [24,35,36,72–75]

$$\begin{aligned} \mathcal{L} = & \bar{\psi}_i \{ i\gamma^\mu \partial_\mu - M^* \} \psi_i + \frac{1}{2} \partial^\mu \sigma \partial_\mu \sigma \\ & - \frac{1}{2} m_\sigma^2 \sigma^2 - \frac{1}{3} g_2 \sigma^3 - \frac{1}{4} g_3 \sigma^4 - g_s \bar{\psi}_i \psi_i \sigma \\ & - \frac{1}{4} \Omega^{\mu\nu} \Omega_{\mu\nu} + \frac{1}{2} m_\omega^2 \omega^\mu \omega_\mu - g_\omega \bar{\psi}_i \gamma^\mu \psi_i \omega_\mu \\ & - \frac{1}{4} \vec{B}^{\mu\nu} \cdot \vec{B}_{\mu\nu} + \frac{1}{2} m_\rho^2 \vec{\rho}^\mu \cdot \vec{\rho}_\mu - g_\rho \bar{\psi}_i \gamma^\mu \vec{\tau} \psi_i \cdot \vec{\rho}^\mu \\ & - \frac{1}{4} F^{\mu\nu} F_{\mu\nu} - e \bar{\psi}_i \gamma^\mu \left(\frac{1 - \tau_{3i}}{2} \right) \psi_i A_\mu. \end{aligned} \quad (1)$$

The mesons σ , ω , and ρ have their respective masses (m_σ , m_ω , m_ρ) and coupling constants (g_s , g_ω , g_ρ). The Dirac spinor, isospin, and its third component are denoted as ψ_i , τ , and τ_3 , respectively. Parameters g_2 , g_3 , and $\frac{e^2}{4\pi}$ are the coupling constants of the nonlinear terms. Also M^* and A_μ stands for the mass of nucleon as well as the photon field respectively. The field tensors for ω^μ , $\vec{\rho}_\mu$, and A_μ fields are denoted as

$$\Omega_{\mu\nu} = \partial_\mu \omega_\nu - \partial_\nu \omega_\mu, \quad (2)$$

$$\vec{B}^{\mu\nu} = \partial_\mu \vec{\rho}_\nu - \partial_\nu \vec{\rho}_\mu, \quad (3)$$

$$F^{\mu\nu} = \partial_\mu A_\nu - \partial_\nu A_\mu, \quad (4)$$

in the respective order of sequence. From Eq. (1), the field equations are obtained in terms of nucleons and

mesons

$$\begin{aligned} [-i\alpha \nabla + \beta(M^* + g_\sigma \sigma) + g_\omega \omega + g_\rho \tau_3 \rho_3] \psi_i &= \epsilon_i \psi_i, \\ (-\nabla^2 + m_\sigma^2) \sigma(r) &= -g_\sigma \rho_s(r) - g_2 \sigma^2(r) - g_3 \sigma^3(r), \\ (-\nabla^2 + m_\omega^2) V(r) &= g_\omega \rho(r), \\ (-\nabla^2 + m_\rho^2) \rho(r) &= g_\rho \rho_3(r). \end{aligned} \quad (5)$$

A numerical solution is then carried out for the meson fields by considering stationary baryonic media, the resultants of which describe the nucleon-nucleon potential [35,54,76] and references therein. The form of the potential for NL3* parameter set with the single-nucleon exchange effect (J_{00}) can be expressed as [24,53,77],

$$\begin{aligned} V_{\text{eff}}^{\text{R3Y}}(r) = & \frac{g_\omega^2}{4\pi} \frac{e^{-m_\omega r}}{r} + \frac{g_\rho^2}{4\pi} \frac{e^{-m_\rho r}}{r} - \frac{g_\sigma^2}{4\pi} \frac{e^{-m_\sigma r}}{r} \\ & + \frac{g_2^2}{4\pi} r e^{-2m_\sigma r} + \frac{g_3^2}{4\pi} \frac{e^{-3m_\sigma r}}{r} + J_{00}(E) \delta(s). \end{aligned} \quad (6)$$

The M3Y (which consist of Michigan-3-Yukawa having 0.25-fm medium-range attractive part, 0.4-fm short-range repulsive part, and 1.414-fm long-range tail of one-pion exchange potential, OPEP) proceeds from the fitting of G -matrix elements predicated on Reid-Elliott soft-core NN interaction [53] in an oscillator basis. The M3Y plus the exchange term takes the form,

$$V_{\text{eff}}^{\text{M3Y}}(r) = 7999 \frac{e^{-4r}}{4r} - 2134 \frac{e^{-2.5r}}{2.5r} + J_{00}(E) \delta(s). \quad (7)$$

The nuclear interaction potential $V_n(R)$ is calculated here within the double-folding approach [53] by using the both M3Y [in Eq. (7)] and R3Y [in Eq. (6)] nucleon-nucleon potential. The expression for the nuclear potential is given as

$$V_n(R) = \int \rho_c(\vec{r}_c) \rho_d(\vec{r}_d) V_{\text{eff}}(|\vec{r}_c - \vec{r}_d + \vec{R}| \equiv r) d^3 r_c d^3 r_d. \quad (8)$$

Here ρ_c and ρ_d are the densities of the emitted cluster (c) and the daughter nuclei (d) respectively. The cluster-daughter total interaction potential is the sum of the nuclear potential $V_n(R)$ and the Coulomb potential $V_C(R) = \frac{Z_c Z_d}{R} e^2$. This potential will be used in the calculation of the WKB penetration probability with the preformed-cluster-decay model.

B. Preformed-cluster-decay model (PCM)

The decay constant and decay half-life in the PCM are given as [7,34]

$$\lambda = \nu_0 P_0 P, \quad T_{1/2} = \frac{\ln 2}{\lambda}. \quad (9)$$

The clusters are assumed to be preborn within the parent nucleus, with preformation probability P_0 hitting the barrier with impinging frequency ν_0 , and penetrate it with penetrability P . It was reported [34] that ν_0 has an approximate constant value of 10^{21} s^{-1} in all the cluster decay studies. It is expressed as

$$\nu_0 = \frac{\text{velocity}}{R_0} = \frac{\sqrt{2E_c/\mu}}{R_0}. \quad (10)$$

Here R_0 represents the radius of the parent nucleus and E_c denotes the kinetic energy of the emitted cluster. As an essential feature of cluster radioactivity, the decay products (daughter nuclei and emitted clusters) are formed in the ground state and the total kinetic energy necessary for the decay process is the Q value ($Q = E_d + E_c$), is shared among both the fragments such that the kinetic energy of emitted cluster $E_c = \frac{A_d}{A} Q$ and $E_d (= Q - E_c)$ is the recoil energy of the daughter nucleus. The Q values are calculated using the ground-state binding energies from the expression

$$Q = BE_p - (BE_d + BE_c), \quad (11)$$

where BE_p , BE_d , and BE_c are the binding energies of the parent, daughter nuclei, and the emitted cluster, respectively.

1. Emergence of neck within the PCM

In Ref. [7], the nuclei are treated as spheres where P_0 and P were theoretically estimated at the touching radius $R = R_t = R_a$, i.e., cluster formation starts at the first classical turning point $V(R_a) \approx Q + E_{\text{vib}}$, where E_{vib} is zero-point vibrational energy, and it appears that the overlapping region ($R_0 \leq R \leq R_t$) of the daughter nuclei and cluster was not taken into account. However, a subsequent investigation [78] revealed that this region (of neck configuration) and the supposed deformations have been duly compensated via the assumption of sphericity of nuclei. Yet, the effect of the neck region will be appraised since it has been demonstrated [37,78] to significantly influence the nuclear proximity potential $V_n(R)$ and is recommended for cluster radioactive-decay data. In the present study, it is assumed that the first turning point emerges at an extended configuration ($R_a \geq R_t$). This obliterates the consideration of potential $V(R < R_a)$ and consequently undermines the shell effect within the barrier, which is not so substantial although it could be easily reckoned by employing the two center shell model (TCSM) [78]. The relative separation distance (ΔR) between two outgoing nuclei is supposed to incorporate the neck formation effects between them and hence is referred to as the neck length. Thus, the first turning point can be defined as $R_a = R_t + \Delta R$. The introduction of the neck is similar to those of the scission point [79] and saddle point [80,81] in statistical fission models. As a step further, rather than using a fixed length for the neck parameter $\Delta R = (0.5, 1.0)$ fm in [37], ΔR will be varied up to 2.0 fm (the limit of nuclear proximity potential). The impact of the expected shift in $V_n(R)$ will be investigated on the decay half-life ($\log_{10} T_{1/2}$). It is to be noted here that the minimum value of the neck length also depends on the Q value of the reaction. As the potential at the first turning point, i.e., $V(R_a)$, should be greater than the Q value for the reaction to take place and as defined above the first turning point R_a depends on ΔR , which can be adjusted to get higher potential with regard to the Q value.

2. Tunneling of the Interaction barrier

The cluster tunnels through the interaction potential $V(R)$ which commences from the first turning point $R = R_a$ and emerges out at second turning point $R = R_b$ such that $V(R_b) = Q$ for ground-state decays (as shown the inset of Figs. 1 and 2).

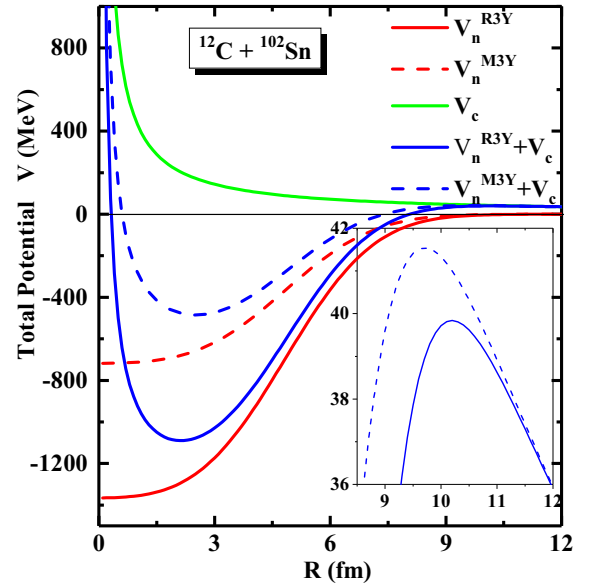


FIG. 1. The profile of total nucleus-nucleus interaction potential V (MeV) and its components, namely, nuclear and Coulomb potential as a function of radial separation for R3Y (NL3*) and M3Y, NN potential for a representative case of $^{114}\text{Ba} \rightarrow ^{12}\text{C} + ^{102}\text{Sn}$. The inset shows a magnified view of the barrier height and position.

Also, $V(R_a) = Q + E_i$, where E_i is the energy that was considered [7] to represent the decay into the excited states of the daughter nucleus or cluster or both. At $R = R_0$, i.e., the radius of the parent nucleus, the potential of the system is equal to its Q value. However, as the parent nucleus becomes unstable, its shape changes, clusters start separating, and consequently

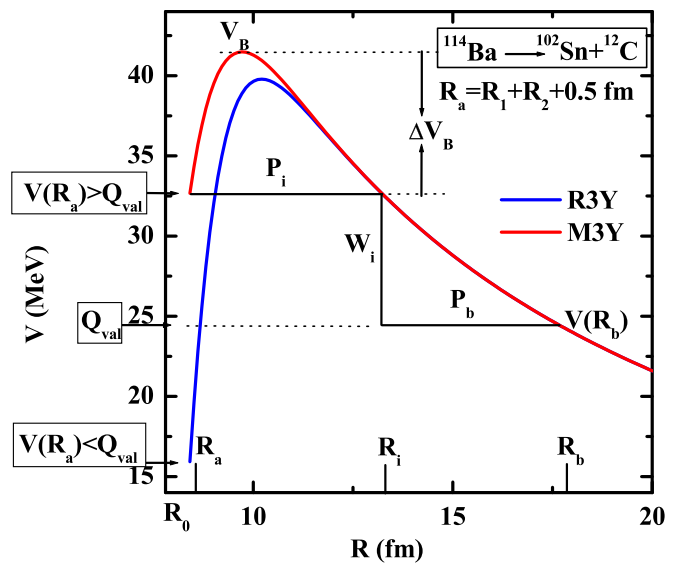


FIG. 2. Comparison between the total interaction potential for both R3Y and M3Y NN potentials for a representative case of $^{114}\text{Ba} \rightarrow ^{12}\text{C} + ^{102}\text{Sn}$. The condition $V(R_a) > Q_{\text{val}}$ must be satisfied to obtain the WKB penetration probability, i.e., the penetration path between the two classical turning points R_a and R_b [see Eqs. (13) and (14)].

a neck is formed. In order to penetrate through the interaction barrier, three steps are involved, as shown in Fig. 2: (a) the penetrability P_i from R_a to R_i , (b) the (inner) de-excitation probability W_i at R_i , taken as one, i.e., $W_i = 1$, which for heavy cluster decays following the excitation model of Greiner and Scheid [82], and (c) the penetrability P_b from R_i to R_b , which leads to the penetration probability as

$$P = P_i P_b, \quad (12)$$

where P_i and P_b are the integrals in the WKB approximation and are given as

$$P_i = \exp\left(-\frac{2}{\hbar} \int_{R_a}^{R_i} \{2\mu[V(R) - V(R_i)]\}^{1/2} dR\right), \quad (13)$$

and

$$P_b = \exp\left(-\frac{2}{\hbar} \int_{R_i}^{R_b} \{2\mu[V(R_i) - Q]\}^{1/2} dR\right), \quad (14)$$

where μ is the reduced mass given by $\mu = A_d A_c / (A_d + A_c)$. The above integrals in Eqs. (13) and (14) are solved numerically.

3. Preformation probability of the cluster

Further in the PCM, it is assumed that both daughter nuclei and cluster are formed at the ground state (g.s.) with a certain preformation probability P_0 . The preformation factor P_0 assimilates the structural properties of the decaying parent nucleus. In the microscopic framework, obtaining the exact value of P_0 could be tedious due to the complexity associated with the nuclear many-body problem. On the other hand, P_0 in cluster decay could be some order of magnitude below unity [24–26,83]. So to estimate the preformation probability (P_0) for the cluster decay, the phenomenological scaling factor proposed by Blendowske and Walliser [64] is used in the present work and is given by

$$P_0 = (P_0^\alpha)^{(A_c-1)/3}, \quad (15)$$

where

$$P_0^\alpha(\text{even}) = 6.3 \times 10^{-3} \quad \text{and} \quad P_0^\alpha(\text{odd}) = 3.2 \times 10^{-3}$$

for $A_c \leq 28$ and slightly increases at $A_c > 28$ [78] after which it becomes slightly constant towards $A_c = 34$ (as shown in Fig. 13 of Ref. [34]). However, some of the clusters under study (in the g.s.) have masses $A_c > 28$. This necessitates a thorough examination of the calculated values from the well-known Blendowske and Walliser phenomenological P_0 scaling factor. Thus, we have adopted the Q -value-based formula [65,66] for the estimation of the preformation factor. It is shown in these references that, among others, this formula gives better predictions of the experimental half-lives of heavy cluster emissions. The Q -value-based formula takes the expression

$$\log P_0 = aQ + bQ^2 + c, \quad (16)$$

where $a = -0.25736$, $b = 6.37291 \times 10^{-4}$, and $c = 3.35106$. Q refers to the liberated energy in the decay process.

III. CALCULATIONS AND DISCUSSIONS

In this section, the cluster decay half-lives of even-even $^{112-122}\text{Ba}$ isotopes in both ground and intrinsic excited states are investigated within the preformed-cluster-decay model (PCM). The nuclear potential (see Fig. 1) of the interacting nuclei is obtained within the relativistic mean-field (RMF) approach with NL3* parameter set. The calculated RMF densities are folded using the relativistic R3Y and phenomenological M3Y interaction potentials using the double-folding technique. The Q values are estimated using the binding energy from the RMF (NL3*) denoted by (Q_{RMF}). For the sake of comparison, the Q values from the experiments [70,84] (Q_{Expt}) and finite-range droplet model (FRDM) [71] (Q_{FRDM}) are employed in the calculation of ground-state cluster radioactivity. The binding energies of a few clusters, with $Z < 8$ are unavailable in the case of FRDM [71], where we have used experimental binding energy to obtain the Q value of the associated decay systems. In the present analysis, our calculation extends to the cluster radioactivity of the parent in the excited state, where the parent emits cluster and daughter to their ground state. In order to obtain the Q values of such a system, the binding energy of the excited state of the parent is used. So far, only the lower limit of ^{114}Ba cluster radioactivity is experimentally observed among the considered isotopic chain of $^{112-122}\text{Ba}$. The decay half-lives are calculated with first turning point at $R_a = R_1 + R_2 + \Delta R = R_t + \Delta R$. Although in earlier studies [37,38,85] by one of us (R.K.) and collaborators, the notion held is that neck-length parameter $\Delta R = 0.5$ fm is the suitable choice for cluster radioactive decay using the nuclear proximity potential. Here, the value $\Delta R = 0.5$ fm is not suitable for the nuclear interaction potential from R3Y NN potential and their corresponding Q values. Hence, we calculate the decay half-lives by adopting two different neck lengths, $\Delta R = 0.5$ and 1.0 fm (see Table I). The higher value of the neck-length parameter for R3Y NN potential can be correlated with its extended repulsive core as compared to the proximity potential. A more detailed analysis of this direction will be communicated shortly.

Figure 1 shows the variation of nuclear potential (V_n), obtained from RMF using recently developed R3Y (NL3*) and relatively older phenomenological M3Y interaction for an illustrative case of $^{12}\text{C} + ^{102}\text{Sn}$, as a function of radial distance R (fm). The Coulomb potential is also shown in the figure for the same interaction system. The inset of this figure shows the turning point of the total potential, which is the sum of nuclear and Coulomb potential (V_c). It is evident from this figure that the nuclear potential corresponding to R3Y (NL3*) is more attractive as compared to that for M3Y. The same is reflected in the total potential as well, where R3Y (NL3*) gives a lower interaction barrier. Once the interaction potential is estimated, we then proceed to the calculation of decay half-life within the PCM. In PCM, the three-step penetration of interaction potential is considered, which is explained in Fig. 2 along with the relevance of ΔR with regard to the Q value of the decay. The three-step involves penetration of barrier at first turning point R_a up to the point R_i , de-excitation ($W_i = 1$) from $V(R_i)$ to Q value and finally penetration from R_i to R_b such that

TABLE I. Comparison between the predictions of the penetration probability P obtained from the WKB approximation for R3Y and M3Y NN potentials using the Q values from the relativistic mean field for NL3* parameter set at neck length $\Delta R = 0.5$ fm. The Q values from the finite-range-droplet model (FRDM) [71] and experiments [70,84] are also used to estimate the penetration probability P for both M3Y and R3Y potential. The last three columns are exclusively for R3Y predictions of the penetration probability at $\Delta R = 1.0$ fm. The explanation for the extended neck length, i.e., $\Delta R = 1.0$ fm for R3Y potential can be found in the footnote of the table and text.

Systems		Penetrability P ($\Delta R = 0.5$ fm) Used Q values for calculation			Penetrability P ($\Delta R = 1.0$ fm) Used Q values for calculation		
		Expt	FRDM	RMF	Expt	FRDM	RMF
$^{112}\text{Ba} \rightarrow ^{76}\text{Sr} + ^{36}\text{Ar}$	R3Y		1.02×10^{-47}	1.57×10^{-45}		2.53×10^{-42}	2.02×10^{-38}
	M3Y		5.10×10^{-47}	7.44×10^{-43}			
$^{112}\text{Ba} \rightarrow ^{100}\text{Sn} + ^{12}\text{C}$	R3Y					1.57×10^{-13}	1.03×10^{-09}
	M3Y		2.14×10^{-14}	1.82×10^{-09}			
$^{112}\text{Ba} \rightarrow ^{98}\text{In} + ^{14}\text{N}$	R3Y					3.49×10^{-33}	5.42×10^{-32}
	M3Y		1.37×10^{-35}	2.48×10^{-34}			
$^{112}\text{Ba}^* \rightarrow ^{103}\text{Sn} + ^9\text{C}$	R3Y			$1.21 \times 10^{-52\text{a}}$			$1.28 \times 10^{-54\text{a}}$
	M3Y			$6.78 \times 10^{-60\text{a}}$			
$^{112}\text{Ba}^* \rightarrow ^{95}\text{Pd} + ^{17}\text{Ne}$	R3Y						$3.05 \times 10^{-21\text{a}}$
	M3Y			$7.02 \times 10^{-25\text{a}}$			
$^{114}\text{Ba} \rightarrow ^{79}\text{Y} + ^{35}\text{Cl}$	R3Y	5.59×10^{-43}	2.90×10^{-42}	2.01×10^{-40}	8.90×10^{-37}	1.39×10^{-35}	3.84×10^{-32}
	M3Y	7.22×10^{-41}	1.46×10^{-39}	9.25×10^{-36}			
$^{114}\text{Ba} \rightarrow ^{102}\text{Sn} + ^{12}\text{C}$	R3Y				2.19×10^{-18}	2.38×10^{-15}	5.87×10^{-11}
	M3Y	8.07×10^{-20}	1.32×10^{-16}	8.32×10^{-12}			
$^{114}\text{Ba}^* \rightarrow ^{105}\text{Sn} + ^9\text{C}$	R3Y			$3.06 \times 10^{-82\text{a}}$			$1.12 \times 10^{-87\text{a}}$
	M3Y			$2.83 \times 10^{-93\text{a}}$			
$^{114}\text{Ba}^* \rightarrow ^{96}\text{Pd} + ^{18}\text{Ne}$	R3Y						$9.71 \times 10^{-13\text{a}}$
	M3Y			$1.66 \times 10^{-14\text{a}}$			
$^{116}\text{Ba} \rightarrow ^{81}\text{Y} + ^{35}\text{Cl}$	R3Y	8.09×10^{-47}	1.18×10^{-44}	2.42×10^{-45}	4.70×10^{-39}	3.14×10^{-33}	1.28×10^{-35}
	M3Y	1.97×10^{-43}	3.81×10^{-37}	9.76×10^{-40}			
$^{116}\text{Ba} \rightarrow ^{104}\text{Sn} + ^{12}\text{C}$	R3Y				5.07×10^{-22}	1.37×10^{-19}	2.27×10^{-17}
	M3Y	1.31×10^{-23}	5.03×10^{-21}	1.23×10^{-18}			
$^{116}\text{Ba}^* \rightarrow ^{104}\text{In} + ^{12}\text{N}$	R3Y			$2.65 \times 10^{-54\text{a}}$			$1.96 \times 10^{-57\text{a}}$
	M3Y			$1.15 \times 10^{-62\text{a}}$			
$^{116}\text{Ba}^* \rightarrow ^{103}\text{Cd} + ^{13}\text{O}$	R3Y			$3.95 \times 10^{-38\text{a}}$			$6.87 \times 10^{-39\text{a}}$
	M3Y			$9.80 \times 10^{-44\text{a}}$			
$^{118}\text{Ba} \rightarrow ^{76}\text{Kr} + ^{42}\text{Ca}$	R3Y	7.29×10^{-50}		1.15×10^{-52}	2.37×10^{-39}	6.97×10^{-32}	2.68×10^{-45}
	M3Y	3.28×10^{-44}	5.74×10^{-36}	1.22×10^{-50}			
$^{118}\text{Ba}^* \rightarrow ^{106}\text{Sn} + ^{12}\text{C}$	R3Y						$7.17 \times 10^{-21\text{a}}$
	M3Y			$2.95 \times 10^{-22\text{a}}$			
$^{120}\text{Ba} \rightarrow ^{77}\text{Kr} + ^{43}\text{Ca}$	R3Y	9.10×10^{-55}		6.40×10^{-52}	6.44×10^{-52}	2.62×10^{-28}	9.18×10^{-48}
	M3Y	1.04×10^{-57}	3.95×10^{-32}	2.61×10^{-53}			
$^{120}\text{Ba}^* \rightarrow ^{108}\text{Sn} + ^{12}\text{C}$	R3Y						$1.74 \times 10^{-26\text{a}}$
	M3Y			$2.85 \times 10^{-28\text{a}}$			
$^{122}\text{Ba} \rightarrow ^{79}\text{Kr} + ^{43}\text{Ca}$	R3Y	1.11×10^{-59}		1.42×10^{-55}	5.17×10^{-55}	5.89×10^{-26}	3.00×10^{-48}
	M3Y	5.91×10^{-61}	4.49×10^{-29}	9.28×10^{-54}			
$^{122}\text{Ba}^* \rightarrow ^{110}\text{Sn} + ^{12}\text{C}$	R3Y						$1.78 \times 10^{-35\text{a}}$
	M3Y			$1.37 \times 10^{-37\text{a}}$			

^aThe reaction system, where the parent nucleus is in its intrinsic excited state (e.s).

$V(R_b) = Q$ value of the decay. The theoretical details of the procedure of these steps are already mentioned in Sec. II A.

In Fig. 2, the interaction potential for R3Y (NL3*) and M3Y NN potential for ^{12}C decay of ^{114}Ba are shown in blue and red colors respectively. The Q value from RMF for this reaction to occur is 24.46 MeV. The calculated potential $V(R_a)$ at $R_a = R_t + 0.5$ fm for R3Y(NL3*) is 15.93 MeV and for M3Y NN potential is 32.67 MeV. Thus, $V(R_a)$ for R3Y (NL3*) is lower and for M3Y NN potential is higher than the Q value of the decay. For R3Y (NL3*), longer neck length

is required to satisfy the condition of $V(R_a) > Q_{\text{val.}}$. This accounts for most of the unfilled spaces (other than in ^{112}Ba identified with unavailable $Q_{\text{Expt.}}$ data) in Table I where the predicted P values of for both R3Y and M3Y NN interactions at $R_a = R_t + 0.5$ fm are tabulated. Furthermore, the barrier characteristics which include the barrier height V_B and its position R_B along with and first turning point $V(R_a)$ have a significant influence on the cluster decay process. In the PCM framework, the barrier lowering effect is incorporated through the neck-length parameter ΔR . The barrier-lowering

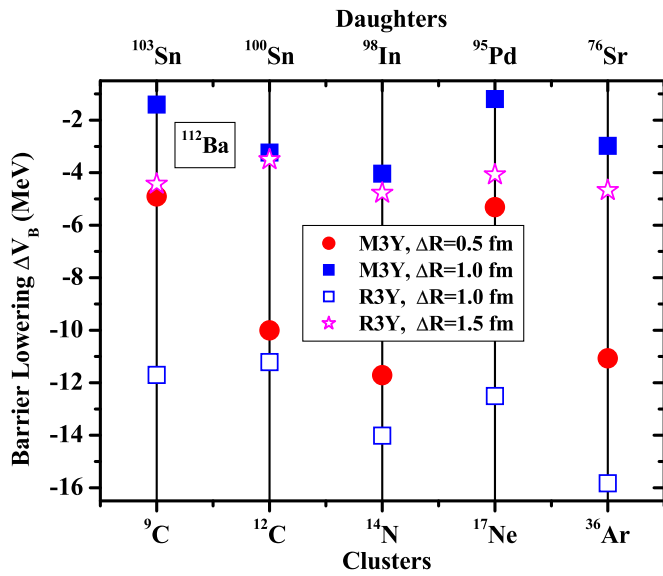


FIG. 3. Variation of barrier lowering parameter ΔV_B (MeV) for ^{12}C , ^{14}N , ^{36}Ar , ^{95}Pd , and ^{103}Sn clusters of ^{112}Ba isotope for different neck-length parameters ΔR from RMF calculations.

parameter ΔV_B which relates $V(R_a)$ to the peak of the barrier V_B , is given by $\Delta V_B = V(R_a) - V_B$ [86].

To see the effect of neck length on the barrier characteristics, we have shown the effect of the barrier-lowering parameter ΔV_B , an inherent feature of PCM, at different values of the neck-length parameter for various clusters, namely, ^9C , ^{12}C , ^{14}N , ^{17}Ne , and ^{36}Ar from the ground and excited states of parent ^{112}Ba nucleus in Fig. 3. The barrier modification for M3Y and R3Y potential is assigned with the solid and open symbols corresponding to a specific cluster. It is to be noted that the barrier lowering parameter ΔV_B is significantly influenced by the changes in the ΔR values. Furthermore, the barrier-lowering parameter is crucial to the determination of the tunneling path as well as the half-life in the cluster decay process. Here the calculation for M3Y and R3Y is shown for the lower value of ΔR at 0.5 and 1.0 fm, respectively. It is observed from Fig. 3 that for both the cases of M3Y and R3Y interaction potentials the ΔV_B increases as the neck parameter value is raised. The same variation of V_B with slightly different magnitudes are observed for all the considered systems, which are not shown in the figure to keep clarity.

The structural information also imparts a significant effect on the study of the decay process and the same can be considered through the preformation probability (P_0). Table II shows the calculated P_0 values as a function of the respective clusters of neutron-deficient $^{112-122}\text{Ba}$ parent nuclei. From the table, it is clear that P_0 values differ from one isotope to another and the mass (which entails the internal structure) of the clusters constitutes the condition around its preformation. Hence, ^{12}C cluster emission follows a similar trend as the others since its preformation [estimated from Eq. (15)] is contingent on its size. Considering the scaling factor of Blendowske and Walliser in Eq. (15) in the decay of each parent nucleus with $A_c \leq 28$ (for systems in the upper panel of the table), the magnitude of the preformation probability P_0 is found to decrease

TABLE II. Calculated preformation probability P_0 for the cluster emissions from $^{112-122}\text{Ba}$ isotopes.

Parent	Cluster	P_0^a Eq. (15) [64]
^{112}Ba	^{12}C	8.53×10^{-09}
	^{14}N	2.91×10^{-10}
	^9C	1.35×10^{-06}
^{114}Ba	^{17}Ne	1.83×10^{-12}
	^{12}C	8.53×10^{-09}
^{116}Ba	^9C	1.35×10^{-06}
	^{18}Ne	3.39×10^{-13}
	^{12}C	8.53×10^{-09}
^{118}Ba	^{12}N	8.53×10^{-09}
	^{13}O	1.58×10^{-09}
^{120}Ba	^{12}C	8.53×10^{-09}
^{122}Ba	^{12}C	8.53×10^{-09}

Parent.	Cluster	Expt.	FRDM	RMF
^{112}Ba	^{36}Ar		8.34×10^{-07}	3.36×10^{-07}
^{114}Ba	^{35}Cl	6.02×10^{-07}	4.43×10^{-07}	1.72×10^{-07}
^{116}Ba	^{35}Cl	9.53×10^{-07}	2.20×10^{-07}	4.12×10^{-07}
^{118}Ba	^{42}Ca	1.08×10^{-07}	1.47×10^{-08}	4.16×10^{-07}
^{120}Ba	^{43}Ca	1.38×10^{-06}	4.71×10^{-09}	6.17×10^{-07}
^{122}Ba	^{43}Ca	2.76×10^{-06}	2.24×10^{-09}	7.74×10^{-07}

^aEstimated from Eq. (15) [64], which is valid for cluster masses $A_c \leq 28$.

^bEstimated from Eq. (16) [65,66], which is adopted for cluster masses $A_c > 28$.

with an increase in the mass of the cluster. In other words, the estimated higher values at smaller cluster sizes which reduce drastically at larger cluster sizes indicate the structure effect. On the other hand, the inclusion of Eq. (16) for systems with $A_c > 28$ (lower panel of the table) departs from the earlier trend since it is based on the Q values (estimated from the RMF and different mass tables). A preformation formula that unifies both mass and decay energy will be communicated shortly.

One of the important quantities used within the PCM to obtain the half-lives of parents in ground and intrinsic excited states is the WKB penetration probability (P). Table I gives the outline of the WKB penetration probabilities of the cluster decay processes for all the considered barium isotopes at neck-length parameter $\Delta R = 0.5$ fm for the Q values from RMF (Q_{RMF}), from FRDM (Q_{FRDM}) [71,84] and from the experiment (Q_{Expt}) [70], for the interacting potential from both R3Y and M3Y NN potentials. One can observe that P is strongly influenced by the choice of Q value as well as the NN interaction employed. From the table, it is obvious that the least values (minima) are formed in ^{12}C decay of all Ba isotopes (yielding daughters in the neighborhood of the doubly magic ^{100}Sn). Hence, the consideration of excitation does not rule out the role of magicity. In the PCM framework, the decay constant λ is directly proportional to the preformation probability P_0 and P . As a result, an increase in the neck-length parameter ΔR should enhance the penetrability. Uniquely, the

TABLE III. Comparison of the decay half-lives for $^{112-122}\text{Ba}$ isotopes calculated for the M3Y and R3Y at $R_a = R_T + 0.5$ fm and for R3Y at $R_a = R_T + 1.0$ fm as well. The Q values are calculated using the binding energies from experimental data (Q_{Expt}) [70], finite-range droplet model (FRDM) data [71] (Q_{FRDM}), and RMF (NL3*) calculated data (Q_{RMF}). However, the unavailable data ($Z < 8$) in Ref. [71] are supplemented by those of Wang *et al.* [84] and distinguished in footnote (a). Q_{Expt} data for ^{112}Ba are unavailable.

Parent nuclei	Daughter nuclei	Emitted cluster	State	Q values (MeV)			$\log_{10} T_{1/2}$								
				Q_{Expt}	Q_{FRDM}	Q_{RMF}	$R_a = R_T + 0.5$ fm			$R_a = R_T + 1.0$ fm					
							M3Y	R3Y	R3Y						
Expt	FRDM	RMF	Expt	FRDM	RMF	Expt	FRDM	RMF	Expt	FRDM	RMF				
^{112}Ba	^{76}Sr	$^{36}\text{Ar}^c$	g.s.		40.75	42.69		30.79	27.01		31.49	29.69		26.09	22.58
	^{100}Sn	^{12}C			22.32 ^a	27.50		0.05	-4.93					-0.82	-4.68
	^{98}In	^{14}N			16.22 ^a	16.61		22.81	21.55			27.16		20.41	19.21
	^{103}Sn	^9C	1st e.s.			8.02 ^b			43.51*			36.25*			38.23*
	^{95}Pd	^{17}Ne	2nd e.s.			31.47 ^b			2.46*						-1.17*
^{114}Ba	^{79}Y	$^{35}\text{Cl}^c$	g.s.	41.45	42.10	44.12	24.77	23.60	20.19	26.88	26.30	24.86	20.68	19.62	16.58
	^{102}Sn	^{12}C		18.99	20.81 ^a	24.46	5.51	2.28	-2.56				4.08	1.02	-3.41
	^{105}Sn	^9C	1st e.s.			5.04 ^b			76.99*			65.96*			71.39*
	^{96}Pd	^{18}Ne	2nd e.s.			39.50 ^b			4.53*						2.76*
^{116}Ba	^{81}Y	$^{35}\text{Cl}^c$	g.s.	40.47	43.60	42.25	27.15	21.48	23.80	30.53	28.99	29.41	22.77	17.56	19.69
	^{104}Sn	^{12}C		17.03	18.20 ^a	19.44	9.32	6.73	4.32				7.74	5.29	3.06
	^{104}In	^{12}N	1st e.s.			10.57 ^b			48.49*			40.12*			43.25*
	^{103}Cd	^{13}O	2nd e.s.			17.06 ^b			30.20*			24.60*			25.36*
^{118}Ba	^{76}Kr	$^{42}\text{Ca}^c$	g.s.	45.14	49.53	42.23	28.89	21.49	34.75	34.54		36.77	24.03	17.41	29.40
	^{106}Sn	^{12}C	1st e.s.			17.49 ^b			7.97*						6.58*
^{120}Ba	^{77}Kr	$^{43}\text{Ca}^c$	g.s.	39.69	52.10	41.39	41.32	18.14	37.26	38.37		35.87	35.52	14.32	31.71
	^{108}Sn	^{12}C	1st e.s.			15.20 ^b			14.02*						12.23*
^{122}Ba	^{79}Kr	$^{43}\text{Ca}^c$	g.s.	38.24	53.80	40.91	44.27	15.41	37.61	43.00		39.43	38.33	12.29	32.10
	^{110}Sn	^{12}C	1st e.s.			12.40 ^b			23.38*						21.27*

^aUnavailable data ($Z < 8$) in Ref. [71] are supplemented by those of Wang *et al.* [84].

^bThe system is in its intrinsic excited state and the corresponding predicted half-life values are marked with asterisk (*).

^cCalculated from Eq. (16) since $A_c > 28$.

penetration probabilities of ^{12}C decays are relatively lower for each considered Ba isotope. This interesting trend will be discussed subsequently.

Table III shows the decay half-life values of 19 predicted clusters in $^{112-122}\text{Ba}$ nuclei [36] in their ground states (g.s.) and intrinsic first (1st e.s.) and second excited states (2nd e.s.), including ^9C , ^{12}C , ^{13}O , $^{12,14}\text{N}$, $^{17,18}\text{Ne}$, ^{35}Cl , ^{36}Ar , and $^{42,43}\text{Ca}$, for different Q values, i.e., from RMF Q_{RMF} , from experiments Q_{Expt} [70], and from FRDM Q_{FRDM} [71,84]. It is important to note that $^{112}\text{Ba} \rightarrow ^{76}\text{Sr} + ^{36}\text{Ar}$ can be regarded as asymmetric fission since the proton masses of both fragments are close. However, the possibility of the emission of heavy clusters such as ^{36}Ar has been predicted in an earlier study [36] which forms the premise for our investigation. Similarly, the reaction agrees with the concept of heavy-particle radioactivity [87,88], although it is mostly identified with heavier systems. Hence, our treatment follows its theoretical prediction [36] since there is no experimental evidence to disprove it. The calculation is also performed for the total interaction potential obtained from both phenomenological M3Y and relativistic R3Y potential at the first turning point $R_a = R_T + 0.5$ fm.

The Q values for the first and second intrinsic excited states of the decaying parents are calculated from the RMF

binding energies and are distinguished with footnote (a) and the corresponding predicted half-life values are marked with an asterisk (*). Here, the term intrinsic stands for the excitation of the parent nucleus that is not induced by temperature but is elicited by its internal vibration and shape degrees of freedom [36,89,90]. Due to unavailable binding energies for the parent nucleus from FRDM and experimental data, there is no comparison made for the systems associated with the first and second excited cluster radioactivity of the parents. A significant increase is noticed in Q values of the 2nd e.s. of $^{112-116}\text{Ba}$ isotopes due to a large difference of about 9–11 MeV in their respective binding energies as compared with those in the 1st e.s. The last three columns feature $R_a = R_T + 1.0$ fm for R3Y (NL3*) for comparison. For tunneling to take place within the WKB framework, it is generally required that the Q values must be positive [91], which indicates an exothermic process $Q > 0$. Besides the unavailable experimental binding energy data for ^{112}Ba from Audi *et al.* [70], the decay half-lives cannot be determined when the potential at touching configuration $V(R_a)$ is less than the Q value of the emitting channel (see Refs. [37,38] for detailed discussion). Thus, one could observe that not all the logarithmic half-life values at $R_a = R_T + 0.5$ fm can be obtained for R3Y NN interaction.

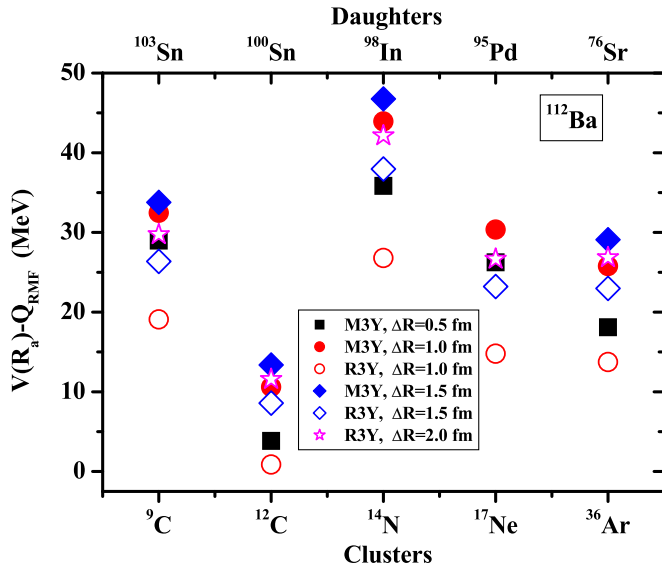


FIG. 4. Variation of the total driving potential $V(R_a) - Q_{\text{RMF}}$ at different neck-length parameter ΔR values. The filled and open symbols are estimated from M3Y and R3Y NN interactions respectively.

We demonstrated the condition $V(R_a) > Q_{\text{val}}$ must satisfy for barrier penetration, i.e., the potential $V(R_a)$ which corresponds to the first turning point R_a must be greater than the Q value. The total driving potential due to the vibrational energy $V(R_a) - Q_{\text{RMF}}$ is the difference between the potential at the first turning point $V(R_a)$ and the energy released during the cluster decay process. Hence, Fig. 4 displays the profile of $V(R_a) - Q$ for cluster ${}^9\text{C}$, ${}^{12}\text{C}$, ${}^{14}\text{N}$, ${}^{17}\text{Ne}$, and ${}^{36}\text{Ar}$ emission of ${}^{112}\text{Ba}$ isotope at different choices of neck-length parameter ΔR from RMF calculations. In this context, the total driving potential must be positive for each reaction system. A similar pattern is maintained in all the cases although some calculations for R3Y at $\Delta R = 0.5$ fm were unsuccessful because $V(R_a) - Q_{\text{RMF}}$ turns out to be negative. As a result, the entrance point is modified by increasing $\Delta R = 1.0$ fm. A similar observation was made at $\Delta R = 2.0$ fm for M3Y where the potential corresponding to the first turning point turns out to be incommensurate with the effective Q value. Following the trend of the color symbols in the figure, all the systems in the ground state manifest similar behavior for each variation in the neck-length values.

Unlike the systems in the ground state where the driving potentials at $\Delta R = 1.5$ fm for RMF are higher than those of M3Y at $\Delta R = 0.5$ fm, it is interesting to note that both systems (associated with ${}^9\text{C}$ and ${}^{17}\text{Ne}$) in their intrinsic excited states manifest a different behavior (easily seen in the color symbols). The deepest minima are observed in the ${}^{12}\text{C}$ cluster. Considering the variation in the neck-length parameter ΔR for M3Y (solid symbols) and R3Y (open symbols) for the first and second intrinsic excited states (having ${}^9\text{C}$ and ${}^{17}\text{Ne}$ clusters, respectively), the driving potential increases with increase in the values of ΔR as in the ground states, such as, for example, where the first and second excited states, in which the solid black square (M3Y at $\Delta R = 0.5$ fm) overlaps

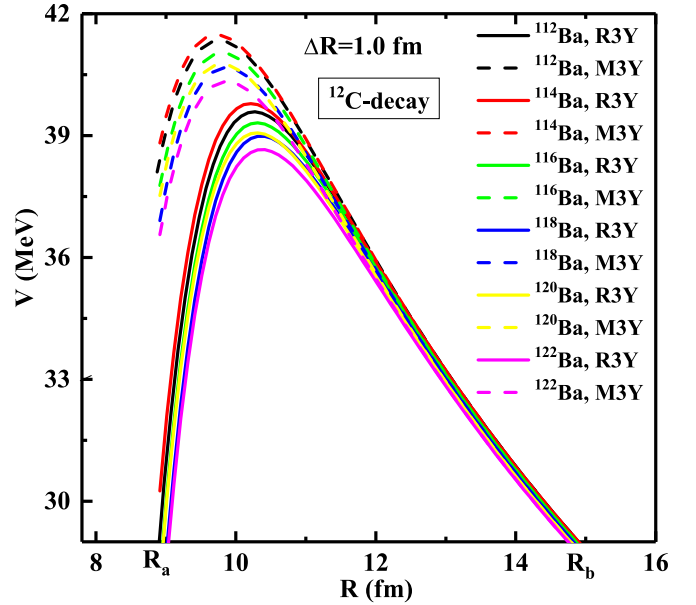


FIG. 5. Interaction potentials estimated for ${}^{12}\text{C}$ decay of $^{112-122}\text{Ba}$ isotopes with a fixed neck-length parameter $\Delta R = 1.0$ fm (i.e., $R_a = R_1 + R_2 + 1.0$ fm) using the RMF calculated values with R3Y (solid lines) and M3Y (dashed lines) NN potentials.

with the open magenta star symbol (R3Y at $\Delta R = 2.0$ fm), a difference of 1.5 fm. On the other hand, in the ground state, the driving potentials for the open magenta star symbol (R3Y at $\Delta R = 2.0$ fm) are (in all cases) very close to those of solid red circle (M3Y at $\Delta R = 1.0$ fm), i.e., a difference of 1.0 fm. Hence, it suggests that the state (ground and excited) of the parent nuclei could considerably influence the neck configuration and hence the corresponding barrier characteristics. Figure 5 shows the variation of interaction potential as a function of R (fm) for the above said ${}^{12}\text{C}$ decays using R3Y (NL3*) and M3Y NN interactions. It is observed from the figure that the barrier is highest for ${}^{114}\text{Ba}$ and lowest for ${}^{122}\text{Ba}$ for both the choices of NN interaction. R_a depict the first turning point for M3Y (dashed lines) and R3Y (solid line) respectively. The difference in the barrier characteristics of M3Y and R3Y potential is manifested in their respective heights.

A keen examination of the cases of ${}^{12}\text{C}$ decays from Table III shows that the values of $\log_{10}(T_{1/2})$ increase from the lightest ${}^{112}\text{Ba}$ to each successive heavier isotope up to ${}^{122}\text{Ba}$. Interestingly, this was uniformly observed in all the Q values for both the interaction potential, namely, M3Y and R3Y NN potentials, wherever the condition $V(R_a) > Q_{\text{val}}$ is satisfied. For example, the $\log_{10} T_{1/2}$ calculated value for RMF at $\Delta R = 0.5$ fm for M3Y is -4.93 for ${}^{12}\text{C}$ decay of $N = Z$ ${}^{112}\text{Ba}$ which increases sequentially (as N/Z increases) up to 23.38 in ${}^{122}\text{Ba}$ isotope. An increase in $\log_{10} T_{1/2}$ values is favored with the increase in the mass number of the emitted clusters. Despite the fact that ${}^{12}\text{C}$ decays occurs in the 1st e.s. of three of the parent nuclei (${}^{118,120,122}\text{Ba}$), the effect of magicity is maintained. However, the inclusion of excitation reduces the half-life values considerably. Also, in all our calculations, ${}^{12}\text{C}$ decay of ${}^{112}\text{Ba}$ has the least $T_{1/2}$ and largest λ .

This phenomenon is due to the extra stability gained in the presence of doubly magic daughter ^{100}Sn ($Z = 50, N = 50$) nuclei and those (Sn) in its vicinity and hence suggest that the structure of the daughter nucleus plays a prominent role in cluster decay processes [92].

The experimental lower limit of $\log_{10}(T_{1/2})$ for ^{12}C decay of ^{114}Ba is found to be 4.10 [23]. Table IV gives a clearer distinction of the half-life predictions between effective R3Y and M3Y NN potentials for ^{12}C decay of ^{114}Ba in comparison with its experimental lower limit. The Q values refer to the available energy for the cluster to undergo tunneling across the potential barrier. Here, prediction of the half-life from the estimated experimental Q value (Q_{Expt}) [70] seem to agree more with the stated experimental lower limit for both R3Y and M3Y NN potentials than those from FRDM (Q_{FRDM}) [71,84] and the calculated RMF Q values (Q_{RMF}). As expected, the experimental Q values brings the calculations closer to the experimental lower limit of half-life. Nonetheless, the predicted value (≈ 1 decimal place) of R3Y potential is relatively closer to this limit. In relation to experimental half-lives, M3Y predicted $\log_{10}(T_{1/2})$ value to be 5.51 s which confirms the assertions in Refs. [37,38] that the fixed neck-length $\Delta R = 0.5$ fm is most suitable in the prediction of decay half-lives. However, R3Y cannot estimate the half-lives at $\Delta R = 0.5$ fm because $V(R_a) < Q_{\text{val}}$, showing that predictions of R3Y reduces by a certain order of magnitude as compared to those of M3Y NN potential. Therefore, we opine that while M3Y can be accurately evaluated at a fixed neck-length $\Delta R = 0.5$ fm, the newly developed R3Y potential should be evaluated at least at $\Delta R = 1.0$ fm to obtain the decay half-lives. The enhancement of the neck parameter ΔR can be connected with the repulsive nature of the relativistic R3Y potential as compared to the phenomenological M3Y NN potential [35].

It is relevant to note from the table that the effective R3Y and M3Y NN potentials accommodate different ranges of ΔR for their barrier penetration. The M3Y NN potentials can conveniently estimate all the half-life values (increasing in proportion with ΔR) between 0.5 and 1.0 fm, while R3Y NN potential thrives well between 1.0 and 1.5 fm. Thus, it becomes necessary to choose an elongated and fixed neck-length (ΔR) value for both M3Y and R3Y in order

to make a meaningful comparison. However, there are still open questions in the choice of the parameter ΔR , which require further investigations. The first turning point R_a is varied from $R_a = R_1 + R_2 = R_t$ to $R_a = R_t + \Delta R$ fitted to the experimental half-life. At $R_a = R_t + 2.0$ fm, the decay half-life for the M3Y NN interaction cannot be estimated since its corresponding potential $V(R_a)$ turns out to be on the right side of the interaction barrier. It is to be noted here that the range of neck length, i.e., $0 \leq \Delta R \leq 2$, relates to the range of nuclear proximity potential [93–95]. This is the reason for which the $\Delta R \geq 2$ fm is usually disregarded in most cluster decay calculations. From our discussion, it is apparent that the neck parameter values, as well as the barrier position, decide the tunneling path as well as the decay half-lives of the respective clusters. Virtually all observations in M3Y and R3Y are uniform except for the difference in the estimated Q values from Table III. The obvious difference in our estimated half-lives is a pointer to the fact that cluster radioactivity half-lives are greatly sensitive to the Q values, neck length, and the effective interaction employed. The sensitivity of decay half-lives to Q values is further illustrated in Fig. 6 and compared to the measured experimental Q value (Q_m^{Exp}), 19.00 MeV (taken from Ref. [96]), at the first turning point $R_a = R_t + 1.0$ fm, which nearly corresponds (shown with green arrow) to the experimental lower limit in Ref. [23]. The difference between the Q_{RMF} and Q_m^{Exp} suggests a need for certain improvements in the prediction and description of the nuclear structure.

Figure 7 shows the logarithmic half-life $\log_{10} T_{1/2}$ for the considered cluster decay of ^{112}Ba calculated from the phenomenological model of Blendowske and Walliser [64] supplemented with the Q -value-based preformation formula of Santhosh and collaborators [65,66] for ^{36}Ar , i.e., $A_c > 28$ using R3Y (in solid black squares) and M3Y (in solid red circles) NN interactions. It is worth mentioning that only the preformation estimated from Q_{RMF} for ^{36}Ar in Table II is used in the present figure for the sake of clarity. Besides the values of M3Y, which were in all cases slightly higher than their corresponding R3Y predictions, and the lowest minima at ^{12}C cluster having a doubly magic daughter, it is observed that among the neighboring nuclei, the logarithmic half-life predictions of the newly developed R3Y agrees more closely with the phenomenological M3Y at this doubly magic

TABLE IV. Comparison between the experimental lower limit of $\log_{10}(T_{1/2})$ for ^{12}C decay of ^{114}Ba and those of three different data sources for M3Y and R3Y NN potential at $\Delta R = (0.5, 1.0, 1.5, \text{ and } 2.0)$ fm. As shown in Table III, Q_{Expt} , Q_{FRDM} , and Q_{RMF} of $^{114}\text{Ba} \rightarrow ^{102}\text{Sn} + ^{12}\text{C}$ have the values 18.99, 20.81, and 24.46 MeV, respectively.

Parent nuclei	Daughter nuclei	ΔR (fm)	R_a (fm)	R3Y			M3Y			Experiment		
				$V(R_a)$ (MeV)	$\log_{10}(T_{1/2})$ (s)		$V(R_a)$	$\log_{10}(T_{1/2})$ (s)				
					Expt	FRDM	RMF		Expt	FRDM	RMF	
^{114}Ba	^{102}Sn	0.5	8.412	15.93	$V(R_a) < Q$			32.67	5.51 ^a	2.28	-2.56	
		1.0	8.912	30.25	4.08 ^b	1.02	-3.41	38.82	6.42 ^a	2.89	-2.61	>4.10 [23]
		1.5	9.412	37.05	5.01 ^a	1.55	-3.80	41.18	-13.40	-13.42	-13.46	
		2.0	9.912	39.50	-13.41	-13.43	-13.47					

^aAgrees with the experimentally observed lower limit in Ref. [23].

^bPredicts the experimentally observed lower limit in Ref. [23] when approximated to one decimal place.

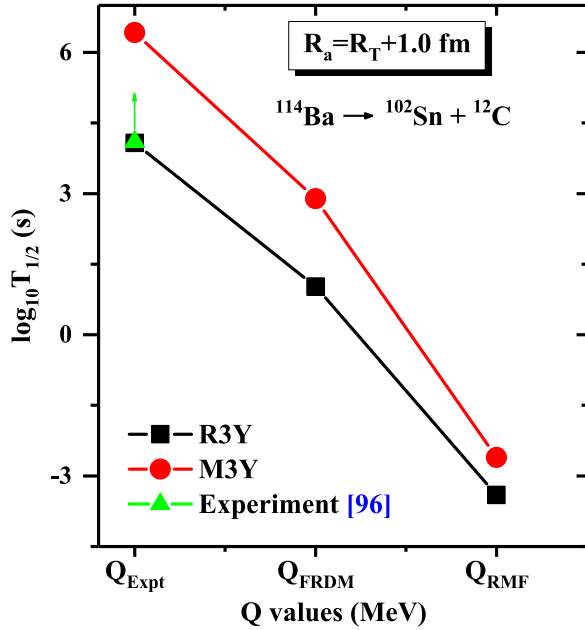


FIG. 6. Sensitivity of half-lives to Q values and comparison between R3Y and M3Y NN potentials with the measured experimental Q value Q_m^{Exp} for ^{114}Ba [96].

shell closure. This observation will be verified in subsequent studies involving other shell closures within the nuclear landscape. To validate our findings, we have compared the Q value (23.17 MeV) of the dinuclear system (DNS) model in Ref. [6] for $^{112}\text{Ba} \rightarrow ^{12}\text{C} + ^{100}\text{Sn}$ to estimate its logarithmic half-life

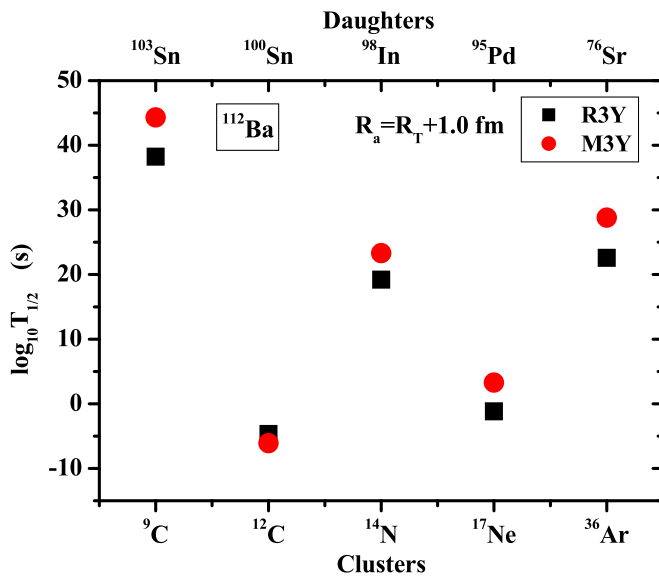


FIG. 7. The Logarithmic half-lives for the considered cluster decays of ^{112}Ba calculated from the phenomenological scaling factor of Blendowske and Walliser [64] supplemented with the Q -value-based preformation formula of Santhosh and collaborators [65,66] for ^{36}Ar (having $A_c > 28$) at first turning point $R_a = R_r + 1.0$ fm for both R3Y and M3Y NN interactions.

(not shown in the graph to avoid the ambiguity of presentation). The $\log_{10} T_{1/2}$ of the mentioned system turns out to be 0.397, which is in better agreement with the prediction of the DNS model [6]. Hence, our study affirms the conclusion of Gao *et al.* [12], who reported that the large difference in cluster decay half-lives can be attributed to the Q values as well as the models employed.

IV. SUMMARY AND CONCLUSIONS

The cluster radioactive decay process of both ground and intrinsic excited states of parent $^{112-122}\text{Ba}$ isotopes is treated as a quantum tunneling effect through a potential barrier in the context of the WKB approximation and the half-lives are deduced within the PCM framework. The popular M3Y density-dependent effective interaction and the recently developed relativistic R3Y potential are employed to obtain the nuclear interaction potential following a double folding procedure. The relativistic mean field with NL3* parameter set is employed for the present analysis in terms of nuclear density, nucleon-nucleon potential, and the Q values of the radioactive system. The results are computed from both M3Y and R3Y NN interactions and compared to the available experimental lower limit (for ^{114}Ba). The Q values of the cluster decay are calculated from the RMF calculations (Q_{RMF}) and results for the ground state are compared with the results for the Q values from the experiments (Q_{Expt}) [70] and the well-known finite-range droplet model (FRDM) predictions (Q_{FRDM}) [71]. We found the barrier height of R3Y is relatively low compared to M3Y, and hence we proposed the least neck-length parameter to accurately predict decay half-lives, which is $\Delta R = 1.0$ fm. The predictions of both potentials are in the limit of the experimental range of acceptance. Nonetheless, it is imperative to conduct further theoretical studies with known experimental half-lives in order to generalize this assertion. From our results, it is evident that the variation in ΔR has significant effects on the decay half-lives and governs the dynamics involved in the decay process. The ^{12}C cluster from $^{112-122}\text{Ba}$ is analyzed and the effect of doubly magic ^{100}Sn is quite apparent, having its half-life lower than other similar cluster decays. Furthermore, it has been demonstrated that the inclusion of excitation does not dominate or rule out the role of magicity. We have given the theoretical estimate of the decay half-lives for various cluster decays from the neutron-deficient Ba isotopes, whose experimental data are not available. This calls for an experimental verification of our findings. It is important to note that our study assumes that the parent, daughter and cluster nuclei are spherical within the RMF framework. The effect of deformation and orientation in the cluster decay in the trans-tin region could influence the estimated $\log_{10} T_{1/2}$. Thus, it is of further interest to incorporate such effects in the future studies.

ACKNOWLEDGMENTS

The authors would like to acknowledge the support from the Fundamental Research Grant Scheme (FRGS) under Grant No. FRGS/1/2019/STG02/UniMAP/02/2 from the Ministry of Education Malaysia, with the Institute

of Engineering Mathematics (IMK) of the Faculty of Applied and Human Sciences UniMAP as the holder. This work was supported by Science Engineering Research

Board (SERB), File No. CRG/2021/001229, FOSTECT Project Code FOSTECT.2019B.04, and FAPESP Project No. 2017/05660-0.

- [1] A. Sandulescu, D. N. Poenaru, and W. Greiner, *Sov. J. Part. Nucl. (Engl. Transl.)* **11**, 6 (1980).
- [2] H. J. Rose and G. A. Jones, *Nature (London)* **307**, 245 (1984).
- [3] D. N. Poenaru, M. Ivascu, A. Sandulescu, and W. Greiner, *J. Phys. G: Nucl. Part. Phys.* **10**, L183 (1984).
- [4] H. F. Zhang, J. M. Dong, G. Royer, W. Zuo, and J. Q. Li, *Phys. Rev. C* **80**, 037307 (2009).
- [5] D. N. Poenaru and W. Greiner, *J. Phys. G: Nucl. Part. Phys.* **17**, S443 (1991).
- [6] S. N. Kuklin, G. G. Adamian, and N. V. Antonenko, *Phys. Rev. C* **71**, 014301 (2005).
- [7] S. S. Malik and R. K. Gupta, *Phys. Rev. C* **39**, 1992 (1989).
- [8] R. Bonetti and A. Guglielmetti, *Rom. Rep. Phys.* **59**, 301 (2007).
- [9] H.-G. Ortlepp, R. Kotte, and F. Stary, in *Proceedings of the 15th International Symposium on Nuclear Physics*, edited by D. Seelinger *et al.* (Nuclear Fission, Gaussing, East Germany, 1985), p. 35.
- [10] M. Balasubramaniam and R. K. Gupta, *Phys. Rev. C* **60**, 064316 (1999).
- [11] D. N. Poenaru, R. A. Gherghescu, and W. Greiner, *J. Phys. G: Nucl. Part. Phys.* **40**, 105105 (2013).
- [12] Y. Gao, J. Cui, Y. Wang, and J. Gu, *Sci. Rep.* **10**, 1 (2020).
- [13] K. P. Santhosh, P. V. Subha, and B. Priyanka, *Pramana* **86**, 819 (2016).
- [14] D. N. Poenaru, R. A. Gherghescu, and W. Greiner, *Phys. Rev. C* **85**, 034615 (2012).
- [15] H. C. Manjunatha and N. Sowmya, *Nucl. Phys. A* **969**, 68 (2018).
- [16] H. C. Manjunatha and N. Sowmya, *Int. J. Mod. Phys. E* **27**, 1850041 (2018).
- [17] D. N. Poenaru, H. Stocker, and R. A. Gherghescu, *Eur. Phys. J. A* **54**, 14 (2018).
- [18] N. Ashok and A. Joseph, *Int. J. Mod. Phys. E* **27**, 1850098 (2018).
- [19] Y. Wang, F. Xing, Y. Xiao, and J. Gu, *Chin. Phys. C* **45**, 044111 (2021).
- [20] Y. T. Oganessian, Y. A. Lazarev, V. L. Mikheev, Y. A. Muzychka, I. V. Shirokovsky, S. P. Tretyakova, and V. K. Utyonkov, *Z. Phys. A* **349**, 341 (1994).
- [21] A. Guglielmetti, R. Bonetti, G. Poli, P. B. Price, A. J. Westphal, Z. Janas, H. Keller, R. Kirchner, O. Klepper, A. Piechaczek *et al.*, *Phys. Rev. C* **52**, 740 (1995).
- [22] A. Guglielmetti *et al.*, *Nucl. Phys. A* **583**, 867 (1995).
- [23] A. Guglielmetti, R. Bonetti, G. Poli, R. Collatz, Z. Hu, R. Kirchner, E. Roeckl, N. Gunn, P. B. Price, B. A. Weaver *et al.*, *Phys. Rev. C* **56**, R2912 (1997).
- [24] B. B. Singh, S. K. Patra, and R. K. Gupta, *Phys. Rev. C* **82**, 014607 (2010).
- [25] B. Singh, S. K. Patra, and R. K. Gupta, *Int. J. Mod. Phys. E* **20**, 1003 (2011).
- [26] Y. Qian and Z. Ren, *J. Phys. G: Nucl. Part. Phys.* **39**, 015103 (2011).
- [27] G. Sawhney, K. Sandhu, M. K. Sharma, and R. K. Gupta, *Eur. Phys. J. A* **50**, 175 (2014).
- [28] Y. L. Zhang and Y. Z. Wang, *Phys. Rev. C* **97**, 014318 (2018).
- [29] D. N. Poenaru, M. Ivascu, A. Sandulescu, and W. Greiner, *Phys. Rev. C* **32**, 572 (1985).
- [30] D. N. Poenaru, W. Greiner, K. Depta, M. Ivascu, D. Mazilu, and A. Sandulescu, *At. Data Nucl. Data Tables* **34**, 423 (1986).
- [31] M. Warda and L. M. Robledo, *Phys. Rev. C* **84**, 044608 (2011).
- [32] M. Warda, A. Zdeb, and L. M. Robledo, *Phys. Rev. C* **98**, 041602(R) (2018).
- [33] Z. Matheson, S. A. Giuliani, W. Nazarewicz, J. Sadhukhan, and N. Schunck, *Phys. Rev. C* **99**, 041304(R) (2019).
- [34] R. K. Gupta and W. Greiner, *Int. J. Mod. Phys. E* **3**, 335 (1994).
- [35] B. B. Sahu, S. K. Singh, M. Bhuyan, S. K. Biswal, and S. K. Patra, *Phys. Rev. C* **89**, 034614 (2014).
- [36] M. Bhuyan, S. K. Patra, P. Arumugam, and R. K. Gupta, *Int. J. Mod. Phys. E* **20**, 1227 (2011).
- [37] R. Kumar, *Phys. Rev. C* **86**, 044612 (2012).
- [38] R. Kumar and M. K. Sharma, *Phys. Rev. C* **85**, 054612 (2012).
- [39] R. K. Gupta, in *Proceedings of the Fifth International Conference on Nuclear Reaction Mechanisms*, edited by E. Gadioli (Ricerca Scientifica ed Educazione Permanente, Milan, 1988), p. 416.
- [40] K. Sharma, G. Sawhney, M. K. Sharma, and R. K. Gupta, *Eur. Phys. J. A* **55**, 1 (2019).
- [41] J. Maruhn and W. Greiner, *Phys. Rev. Lett.* **32**, 548 (1974).
- [42] H. J. Fink, J. Maruhn, W. Scheid, and W. Greiner, *Z. Phys.* **268**, 321 (1974).
- [43] G. Gamow, *Z. Phys.* **51**, 204 (1928).
- [44] C. Eckart, *Phys. Rev.* **35**, 1303 (1930).
- [45] P. H. Quentin and H. Flocard, *Annu. Rev. Nucl. Part. Sci.* **28**, 523 (1978).
- [46] W. H. Hornyak, *Nuclear Structure* (Academic Press, New York, 1975).
- [47] N. Schunck and L. M. Robledo, *Rep. Prog. Phys.* **79**, 116301 (2016).
- [48] J. Okolowicz, W. Nazarewicz, and M. Ploszajczak, *Fortsch. Phys.* **61**, 66 (2013).
- [49] C. Simenel, D. Lacroix, and B. Avez, *Microscopic approaches for nuclear many-body dynamics: applications to nuclear reaction* (VDM Verlag, Sarrebruck, Germany, 2010), arXiv:0806.2714.
- [50] D. Vautherin and D. M. Brink, *Phys. Rev. C* **5**, 626 (1972).
- [51] E. Epelbaum, H.-W. Hammer, and U.-G. Meißner, *Rev. Mod. Phys.* **81**, 1773 (2009).
- [52] A. Ekström, G. Baardsen, C. Forssén, G. Hagen, M. Hjorth-Jensen, G. R. Jansen, R. Machleidt, W. Nazarewicz, T. Papenbrock, J. Sarich, and S. M. Wild, *Phys. Rev. Lett.* **110**, 192502 (2013).
- [53] G. R. Satchler and W. G. Love, *Phys. Rep.* **55**, 183 (1979).
- [54] B. Singh, M. Bhuyan, S. K. Patra, and R. K. Gupta, *J. Phys. G: Nucl. Part. Phys.* **39**, 069501 (2012).
- [55] S. Biswal, M. A. El Sheikh, N. Biswal, N. Yusof, H. Kassim, S. K. Patra, and M. Bhuyan, *Nucl. Phys. A* **1004**, 122042 (2020).
- [56] N. Itagaki, A. V. Afanasjev, and D. Ray, *Phys. Rev. C* **101**, 034304 (2020).

- [57] N. J. A. Awwad, H. Abusara, and S. Ahmad, *Phys. Rev. C* **101**, 064322 (2020).
- [58] M. Dutra, B. M. Santos, and O. Lourenço, *J. Phys. G: Nucl. Part. Phys.* **47**, 035101 (2020).
- [59] A. Taninah, S. E. Agbemava, and A. V. Afanasjev, *Phys. Rev. C* **102**, 054330 (2020).
- [60] B. Singh and M. Kaur, in *Nuclear Structure Physics* (CRC Press, Boca Raton, 2020), pp. 167–183.
- [61] S. O. Allehabi, V. A. Dzuba, V. V. Flambaum, A. V. Afanasjev, and S. E. Agbemava, *Phys. Rev. C* **102**, 024326 (2020).
- [62] B. Wei, Q. Zhao, Z.-H. Wang, J. Geng, B.-Y. Sun, Y.-F. Niu, and W.-H. Long, *Chin. Phys. C* **44**, 074107 (2020).
- [63] Y. Cao, S. E. Agbemava, A. V. Afanasjev, W. Nazarewicz, and E. Olsen, *Phys. Rev. C* **102**, 024311 (2020).
- [64] R. Blendowske and H. Walliser, *Phys. Rev. Lett.* **61**, 1930 (1988).
- [65] K. P. Santhosh and C. Nithya, *Phys. Rev. C* **97**, 064616 (2018).
- [66] K. P. Santhosh and T. A. Jose, *Phys. Rev. C* **99**, 064604 (2019).
- [67] G. Wentzel, *Z. Phys.* **38**, 518 (1926).
- [68] H. A. Kramers, *Z. Phys.* **39**, 828 (1926).
- [69] L. Brillouin, *Compt. Rend. Hebd. Seances Acad. Sci.* **183**, 24 (1926).
- [70] G. Audi, A. H. Wapstra, and C. Thibault, *Nucl. Phys. A* **729**, 337 (2003).
- [71] P. Möller, A. J. Sierk, T. Ichikawa, and H. Sagawa, *At. Data Nucl. Data Tables* **109–110**, 1 (2016).
- [72] C. J. Horowitz and B. D. Serot, *Nucl. Phys. A* **368**, 503 (1981).
- [73] B. D. Serot and J. D. Walecka, *Adv. Nucl. Phys.* **16**, 1 (1986).
- [74] P. Ring, *Prog. Part. Nucl. Phys.* **37**, 193 (1996).
- [75] M. Bhuyan, *Phys. Rev. C* **92**, 034323 (2015).
- [76] M. Bhuyan, R. Kumar, S. Rana, D. Jain, S. K. Patra, and B. V. Carlson, *Phys. Rev. C* **101**, 044603 (2020).
- [77] D. Basu, *J. Phys. G: Nucl. Part. Phys.* **29**, 2079 (2003).
- [78] S. Kumar and R. K. Gupta, *Phys. Rev. C* **55**, 218 (1997).
- [79] T. Matsuse, C. Beck, R. Nouicer, and D. Mahboub, *Phys. Rev. C* **55**, 1380 (1997).
- [80] S. J. Sanders, *Phys. Rev. C* **44**, 2676 (1991).
- [81] S. J. Sanders, D. G. Kovar, B. B. Back, C. Beck, D. J. Henderson, R. V. F. Janssens, T. F. Wang, and B. D. Wilkins, *Phys. Rev. C* **40**, 2091 (1989).
- [82] M. Greiner and W. Scheid, *J. Phys. G: Nucl. Phys.* **12**, L229 (1986).
- [83] C. Phookan, *Chin. J. Phys.* **55**, 176 (2017).
- [84] M. Wang, G. Audi, A. H. Wapstra, F. G. Kondev, M. MacCormick, X. Xu, and B. Pfeiffer, *Chin. Phys. C* **36**, 1603 (2012).
- [85] N. K. Virk, R. Kumar, and M. K. Sharma, *Eur. Phys. J. A* **56**, 35 (2020).
- [86] K. Sharma and M. K. Sharma, *Int. J. Mod. Phys. E* **28**, 1950048 (2019).
- [87] D. N. Poenaru, R. A. Gherghescu, and W. Greiner, *Phys. Rev. Lett.* **107**, 062503 (2011).
- [88] G. R. Sridhar, H. C. Manjunatha, N. Sowmya, P. S. Damodara Gupta, and H. B. Ramalingam, *Eur. Phys. J. Plus* **135**, 291 (2020).
- [89] M. Bhuyan, *Phys. At. Nucl.* **81**, 15 (2018).
- [90] S. K. Patra, M. Bhuyan, M. S. Mehta, and R. K. Gupta, *Phys. Rev. C* **80**, 034312 (2009).
- [91] N. S. Rajeswari, K. R. Vijayaraghavan, and M. Balasubramaniam, *Eur. Phys. J. A* **47**, 1 (2011).
- [92] K. Wei and H. F. Zhang, *Phys. Rev. C* **96**, 021601(R) (2017).
- [93] R. K. Gupta, in *Clusters in Nuclei*, Lecture Notes in Physics Vol. 818, edited by C. Beck (Springer-Verlag, Berlin, 2010), Vol. I, p. 223.
- [94] Niyti, G. Sawhney, M. K. Sharma, and R. K. Gupta, *Phys. Rev. C* **91**, 054606 (2015).
- [95] R. K. Gupta, S. K. Arun, R. Kumar, and Niyti, *Int. Rev. Phys. (IREPHY)* **2**, 369 (2008).
- [96] C. H. Mazzocchi, Z. Janas, L. Batist, V. Belleguic, J. Döring, M. Gierlik, M. Kapica, R. Kirchner, G. A. Lalazissis, H. Mahmud *et al.*, *Phys. Lett. B* **532**, 29 (2002).